Development of a Novel Mesoporous Catalyst UDCaT-6: Kinetics of Synthesis of *tert*-Amyl Methyl Ether (TAME) from *tert*-Amyl Alcohol and Methanol

Ganapati D. Yadav* and Ambareesh D. Murkute

Department of Chemical Engineering, University Institute of Chemical Technology (UICT), University of Mumbai, Matunga, Mumbai - 400 019, India

Received: April 24, 2004; In Final Form: August 10, 2004

UDCaT-6, a novel active mesoporous and stable catalyst, was synthesized by generating in situ nanosized acidic centers of chlorosulfonic acid treated zirconia in the pores of highly ordered hexagonal mesoporous silica (HMS). For the first time, we have used chlorosulfonic acid as a source of sulfating agent to treat zirconia in pores of the HMS. The catalyst is characterized by XRD, FTIR, EDAX, SEM, and BET surface area and pore size analysis, and probe reactions. The structural integrity of HMS is maintained in UDCaT-6. The activity and stability of UDCaT-6 was tested in liquid phase alkylation of toluene with benzyl chloride and vapor phase synthesis of *tert*-amyl methyl ether (TAME) from *tert*-amyl alcohol (TAA) and methanol where corrosive acid HCl and water are generated as biproducts. A complete theoretical and experimental analysis is presented and kinetics are evaluated. The model explains the experimental data very well.

1. Introduction

The limitations of microporous zeolites as catalysts in a variety of reactions involving bulky reactants are well documented. During the past decade, a plethora of work has dealt with the synthesis of mesoporous materials with the incorporation of different functionalities. Among many solid acids other than zeolites, incorporation of superacidity into metal oxides has received considerable attention. Sulfated zirconia is the most extensively studied material due to its superacidic nature.[1] However, some of the major problems associated with sulfated zirconia in the bulk form are its low efficiency due to low surface area (∼100 m^2/g) and its rapid deactivation and relatively poor stability in reactions where water is generated as a coproduct. As an alternative, we synthesized a novel highly acidic mesoporous solid catalyst named UDCaT-1, which is a synergistic combination of S-ZrO_2 and hexagonal mesoporous silica (HMS).[2] (*The acronym UDCaT stands for University Department of Chemical Technology (UDCT), by which our institute was known until recently*). We have brought out the novelties of UDCaT-1 with reference to sulfated zirconia (S-ZrO_2) in a number of industrially relevant reactions.[1a−f] Similarly, UDCaT-2 was a superacidic shape selective catalyst.[1g−j] Sulfuric acid is the most frequently used sulfating agent for the treatment of zirconia. UDCaT-4 was prepared as a novel mesoporous solid acid catalyst via synergism of persulfated alumina and zirconia into HMS.[3a−b] Very recently, we synthesized a novel stable superacidic catalyst UDCaT-5,[3c] for the preparation of which chlorosulfonic acid was used for the first time as a new source for the incorporation of sulfate ions into zirconia. UDCaT-5 contains more sulfate ions without any chloride ions and is more active and stable in comparison with S-ZrO_2. This novel material was fully characterized and it was found to possess a remarkable activity and extraordinary stability in comparison with conventional S-ZrO_2 in a number of reactions. However, the surface area of UDCaT-5 (∼83 m^2/g) is lower than that of S-ZrO_2 (∼100 m^2/g). We thought to synthesize a mesoporous material possessing higher acidity and greater surface area. Thus, the current work deals with synthesis and characterization of a novel material, named UDCaT-6, and its application in the synthesis of *tert*-amyl methyl ether (TAME), a fuel oxygenate, from *tert*-amyl alcohol and methanol. This work covers studies in kinetics of the reaction.

Production of oxygenated fuel additives such as methyl *tert*-butyl ether (MTBE), ethyl *tert*-butyl ether (ETBE), and *tert*-amyl methyl ether (TAME) grew due to their role in making ecofriendly and cleaner burning gasolines. However, MTBE, the fastest growing petrochemical during 1980s, received a setback due to its leakage into groundwater and particularly due to the strong lobbying of ethanol producers in the United States, which ultimately resulted in a ban on its use as a fuel additive in several Western countries. The focus is now shifted to other additives such as TAME and ETBE. The blending Reid vapor pressure (RVP) of TAME (1 psi) is lower than that of MTBE (8 psi) and ETBE (4 psi). TAME has an octane number of 106, which is closer to MTBE's 109. Thus, TAME shows a lot of promise as an alternative to MTBE. The synthesis of TAME has been attempted by several researchers by using a variety of solid acid catalysts.

TAME is synthesized in the liquid phase from isoamylenes and methanol over strongly acidic macroporous ion-exchange resin catalysts in continuous and semibatch mechanically agitated slurry reactors. A single site mechanism for isomerization and a dual site mechanism for etherification of isoamylenes with methanol over ion-exchange fiber SMOPEX-101 have been proposed.[4] Oost and Hoffmann[5] determined the microkinetics of the synthesis of TAME from methanol and a mixture of isoamylenes over Lewatit SPC 118, a macroporous sulfonic acid resin in a continuous flow recycle reactor in the range 50−70 °C at 1.6 MPa. Reactive distillation combined with evaporation has been used to synthesize MTBE and ETBE by a condensation of methanol and ethanol, respectively, with *tert*-

* To whom correspondence should be addressed. Tel.: ++91−22−2410 2121; 2414 5616. Fax: ++91−22−2410 2121; 2414 5614. Email: gdyadav@yahoo.com, gdyadav@udct.org.

10.1021/jp0482060 CCC: $27.50 © 2004 American Chemical Society
Published on Web 10/09/2004

butyl alcohol at atmospheric pressure.[6−8] We have brought out the novelties of ion-exchange resins with reference to other solid acid catalysts such as clays and their modified forms, zeolites, sulfated zirconia, mesoporous solid acid, UDCaT-1, and UDCaT-2 for condensation reactions of alcohols to get different ethers such as MTBE, ETBE, and TAME.[9−14] Synthesis of TAME from *tert*-amyl alcohol and methanol was studied over K-10 clay, 20% w/w dodecatungstatophosphoric acid (DTP) supported on K-10 clay, and several cation exchange resins; Amberlyst-36 was found to be a better catalyst and the reaction follows pseudo-first-order kinetics.[9] Despite their good activity, ion-exchange resins have severe limitations of temperature instability and loss of acid sites due to leaching.[15−19] This has clearly limited their potential applications in high temperature reactions. Many acidic catalysts, such as microporous zeolites, sulfated zirconia (S-ZrO_2), and heteropoly acids (HPAs), have been employed to catalyze similar types of etherification reactions such as MTBE from methanol and *tert*-butanol.[20−24] Zeolites have been investigated as potential alternative catalysts for the synthesis of MTBE. However, most of the zeolites are less efficient than Amberlyst-15[19,25−27] and only β-zeolite is nearly as active as the resin.[28]

The foregoing suggests that there still exists tremendous scope to design and synthesize better catalysts than cation exchange resins for the synthesis of oxygenated fuels. The current research is in that direction.

2. Experimental Section

2.1. Chemicals. Zirconium oxychloride, aqueous ammonia solution, and methanol (all AR grade), 95% w/w ethanol, benzyl chloride, and toluene were procured from M/s. s.d. Fine Chemicals Ltd., Mumbai. The *tert*-amyl alcohol and tetraethyl orthosilicate (TEOS) were procured from Fluka. Chlorosulfonic acid, dodecylamine, and hexadecylamine were obtained from Spectrochem Ltd., Mumbai. Amberlyst-15 was obtained from Rohm and Haas.

2.2. Catalyst Preparation. Zirconium hydroxide was prepared by hydrolysis of aqueous zirconium oxychloride ($ZrOCl_2 \cdot 8H_2O$) with aqueous ammonia at room temperature in the pH range 9−10. The precipitated zirconium hydroxide was washed with deionized water until a neutral filtrate was obtained; the absence of chlorine ion was detected by phenolphthalein and $AgNO_3$ tests. Zirconium hydroxide was dried in an oven for 24 h at 100 °C and crushed to 100 mesh size.

Sulfated zirconia was prepared by immersing $Zr(OH)_4$ in 15 cm^3/g of 0.5 M sulfuric acid followed by drying at 120 °C for 24 h and calcination at 650 °C for 3h.[1a]

UDCaT-5 was prepared by immersing $Zr(OH)_4$ in 15 cm^3/g of 0.5 M solution of chlorosulfonic acid in ethylene dichloride and keeping the $Zr(OH)_4$ in the solution for 5 min. Without allowing moisture absorption, the sample was kept in an oven and heating was started to evaporate the solvent. After 30 min, the temperature was raised to 120 °C, where the sample was maintained for a further 24 h. It was then calcined at 650 °C for 3 h to get the final catalyst, UDCaT-5.[3c]

Hexagonal mesoporous silica (HMS) was prepared as follows. Dodecylamine (5 g) was dissolved in 41.8 g of ethanol and 29.6 g of distilled water. Tetraethyl orthosilicate (20.8 g) was added to it under vigorous stirring. The addition of ethanol improved the solubility of the template. The reaction mixture was aged for 18 h at 30 °C. Clear liquid above the white precipitate was decanted and the precipitate of HMS was dried on a glass plate. The template was removed by calcining the resulting material at 500 °C in air for 3 h.[29]

UDCaT-6 was prepared by adding an aqueous solution of 2.5 g zirconium oxychloride to 5 g precalcined HMS by incipient wetness technique, and this was dried in an oven at 120 °C for 3 h. The dried material was hydrolyzed by ammonia gas and washed with distilled water until no chloride ions were detected, which was confirmed by $AgNO_3$ test. It was further dried in an oven for 2 h at 120 °C. $Zr(OH)_4$/HMS was immersed in 15 cm^3/g of 0.5 M chlorosulfonic acid in ethylene dichloride for 5 min and then, without allowing moisture absorption, it was oven dried to evaporate the solvent at 120 °C. The sample was kept in the oven at 120 °C for a further 24 h and calcined thereafter at 650 °C for 3 h to get the active catalyst UDCaT-6.

2.3. Characterization of Catalysts. Infrared spectra of the samples pressed in KBr pellets were obtained with a Perkin-Elmer instrument at a resolution of 2 cm^{-1} between 4000 and 350 cm^{-1}, and in each case the sample was referenced against a blank KBr pellet.

Powder X-ray diffraction (XRD) patterns were obtained by using Cu Kα radiation (λ = 1.540 562). Samples were step scanned from 1 to 40 in 0.045 steps, with a stepping time of 0.5 s.

Surface area measurements and pore size distributions analysis were done, after pretreating the sample under high vacuum at 300 °C for 4 h, by nitrogen adsorption on a Micromeritics ASAP 2010 instrument at an adsorption temperature of 77 K.

The elemental compositions of HMS and UDCaT-6 were obtained by Energy Dispersive X-ray Spectroscopy (EDXS) on a KEVEX X-ray spectrometer.

Scanning electron micrographs of HMS and UDCaT-6 were taken on a Cameca SU 30 microscope. The dried samples were mounted on specimen studs and sputter coated with a thin film of gold to prevent charging. The gold coated surface was then scanned at various magnifications using the SEM.

2.4. Reaction Procedure and Analysis. Liquid phase alkylation of toluene with benzyl chloride was conducted in a cylindrical glass reactor of 5 cm i.d. and 10 cm height. The reactor had four glass baffles and a four bladed disk turbine impeller located at a height of 0.5 cm from the bottom of the vessel and mechanically agitated with an electric motor at 1000 rpm. Samples were withdrawn periodically and analyzed by a Chemito GC equipped with a 3.8 mm × 4m stainless steel column packed with 10% OV-17 on Chromosorb WHP, as well as with a FID detector.

Vapor phase synthesis of TAME was conducted in a down flow fixed bed Hastelloy HC-276 reactor with a 25.4 mm i.d. and a 300 mm length at atmospheric pressure, equipped with an upstream vaporizer and downstream condenser (Figure 1). The liquid feed containing *tert*-amyl alcohol and methanol was fed by a double piston (Well Chrom HPLC-pump K-120) pump to the vaporizer by using N_2 as a carrier gas at a WHSV of 20 h^{-1}, and the effluent was analyzed online by GC (GC1000 Chemito, Toshniwal Instruments, India) equipped with a 0.22 mm × 25 m capillary column and a FID detector.

In a typical run, 2 g of catalyst was charged to the reactor and stacked between glass beads and ceramic wool. The reactor was maintained under isothermal conditions during all runs and the effects of various parameters such as mole ratio, WHSV, temperature, and W/F_{A_0} (weight of catalyst per unit molar flow

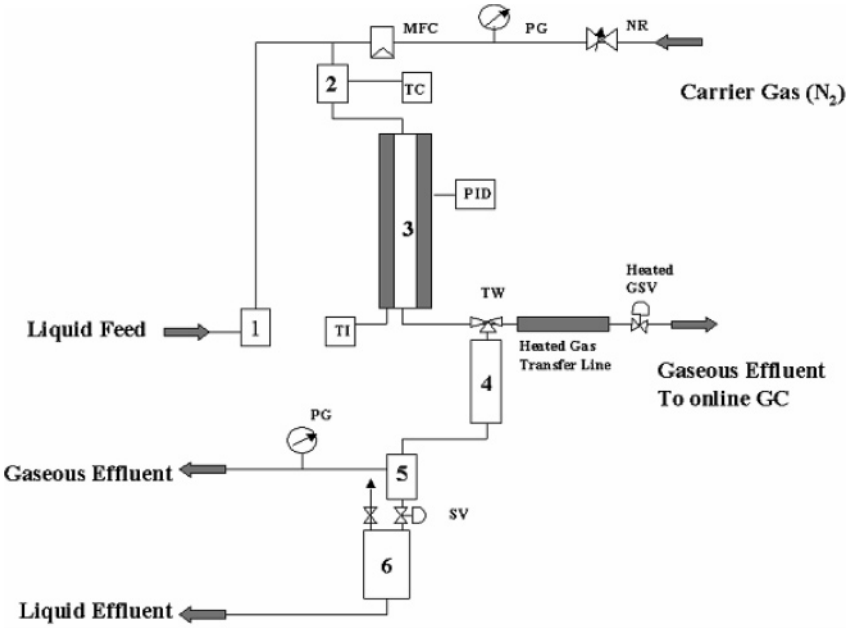

Figure 1. Schematic flow diagram of fixed bed catalytic reactor. (1) Pump; (2) Vaporizor; (3) Reactor; (4) Condenser; (5) Phase separator; (6) Receiver.

SCHEME 1: Condensation of *tert*-amyl alcohol with methanol over solid acid (H^+) over UDCaT-6

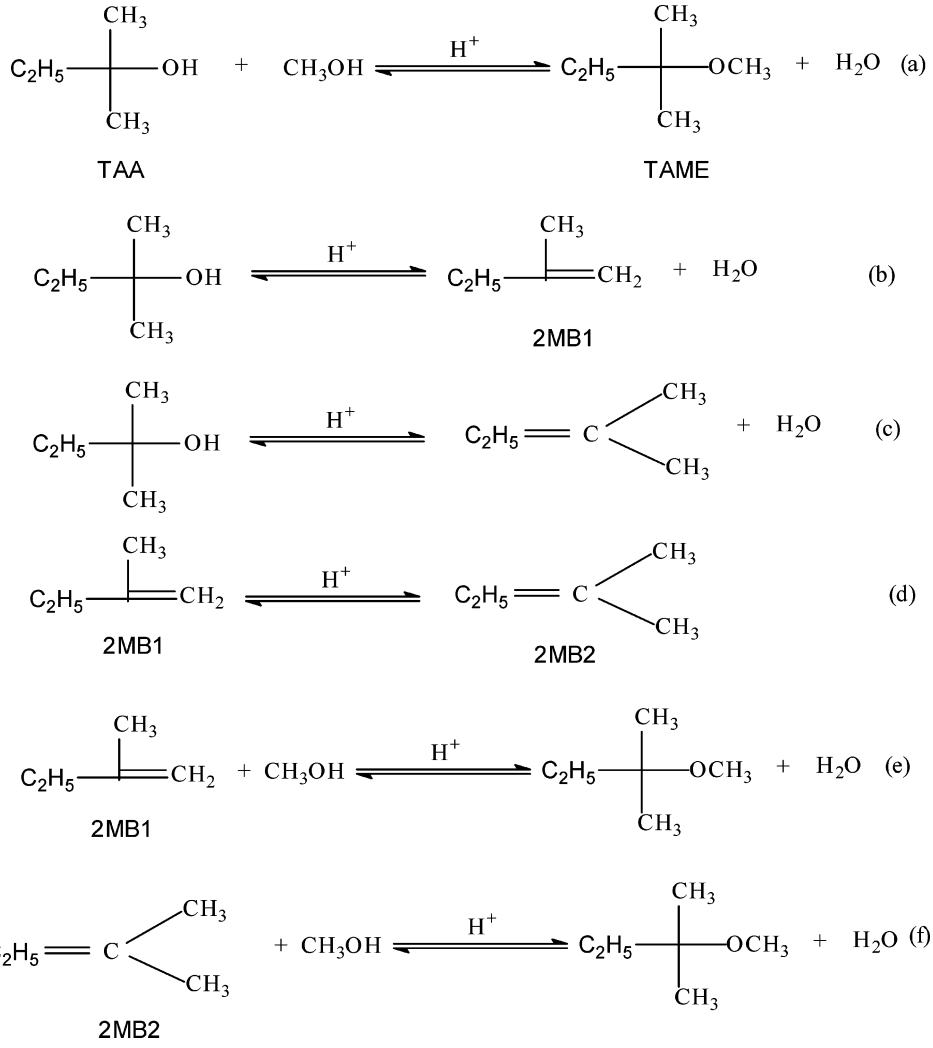

rate of reactant) were studied. A material balance was done to find the amount of water formed from the stoichiometry of the reaction. Water results from the dehydration of alcohol (reactions a, b, and c in Scheme 1).

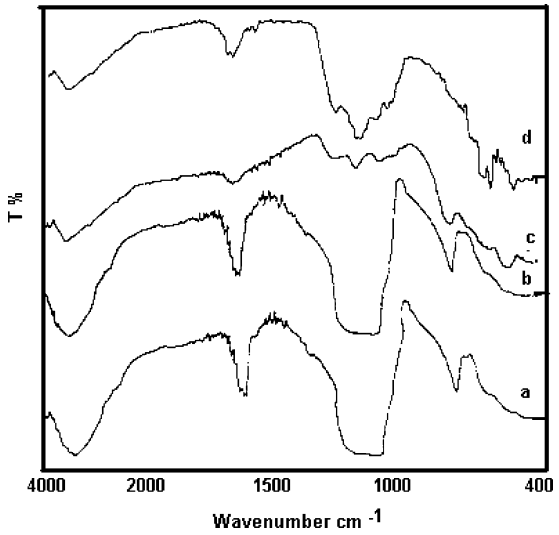

Figure 2. FTIR spectra: (a) HMS; (b) UDCaT-6; (c) S-ZrO_2; (d) UDCaT-5.

3. Results and Discussion

3.1. Characterization. *3.1.1. IR Spectroscopy*. It was expected that, during the calcinations of UDCaT-6, chlorosulfonic acid would decompose to sulfuryl chloride, pyrosulfuryl dichloride, sulfuric acid, sulfur dioxide, chlorine, and water,[30] and sulfur must be retained on the surface of the UDCaT-6. Similar types of results were obtained during synthesis of UDCaT-5.[3c] Thus, FTIR spectroscopy was used to elucidate the nature of the sulfur ion retained on UDCaT-6. The FTIR spectra depict the presence of the characteristic covalent S═O band in the region of 1000−1200 cm^{-1} on UDCaT-6 (Figure 2.). The IR spectra of S-ZrO_2 and UDCaT-5 show a similar pattern to that of UDCaT-6, indicating the presence of the bidentated chelating sulfate group coordinated to zirconia. This band is often responsible for the characteristic superacidity in S-ZrO_2 and UDCaT-5.[1−3] A similar nature of the sulfated group was observed in UDCaT-6. Furthermore, the band at 1631−1642 cm^{-1} is attributed to the δ_{O-H} bending frequency of water molecules associated with the sulfate group,[2,3,31] and it suggests that chlorosulfonic acid decomposes during the calcination of UDCaT-6 and the sulfate ion is retained on the surface of UDCaT-6, which was further corroborated by elemental analysis that will be discussed later. An additional broad band at 3400 cm^{-1} corresponds to the stretching vibration δ_{OH} of the hydroxyl group,[3,31] and it reveals that during calcination at 650 °C, condensation of hydroxyl groups of $Zr(OH)_4$ must be occuring in HMS, leading to a crystalline zirconia without any change of the nature of sulfate species. The retention of sulfur in UDCaT-6 was further confirmed by EDAX and the formation of crystalline zirconia in HMS was further supported by XRD diffraction.

3.1.2. X-ray Diffraction. The structural integrity of HMS, as well as of UDCaT-6, was determined with X-ray diffraction. One diffraction peak in the low angle region ($2\theta = 1-10°$) is visible, indicating that HMS has a long range hexagonal ordering and is also visible in UDCaT-6 (Figure 3A). Both bulk S-ZrO_2 and UDCaT-5 show the presence of the crystalline tetragonal phase of zirconia in the ordinary region ($2\theta = 30$ and 50°) due to incorporation of sulfate ion.[1−3] However, UDCaT-6 shows the reflection of zirconia at $2\theta = 30°$ and $2\theta = 50°$ both having very low and broad intensities (Figure 3B). These diffraction peaks for UDCaT-6 can be attributed to the tetragonal crystalline phase rather than the monoclinic phase of zirconia inside the pores of HMS. The stabilization of the tetragonal phase of zirconia by sulfate ions using sulfuric acid is well known for S-ZrO_2. The case with UDCaT-5 for which chlorosulfonic acid was used as a sulfating agent was similar.[3c] The same phenomenon was also observed in the case of UDCaT-6; it would mean that there was an introduction of sulfate ions through chlorosulfonic acid treatment, which must have stabilized the tetragonal phase of zirconia. FTIR analysis further supports the introduction of sulfate ions in UDCaT-6.

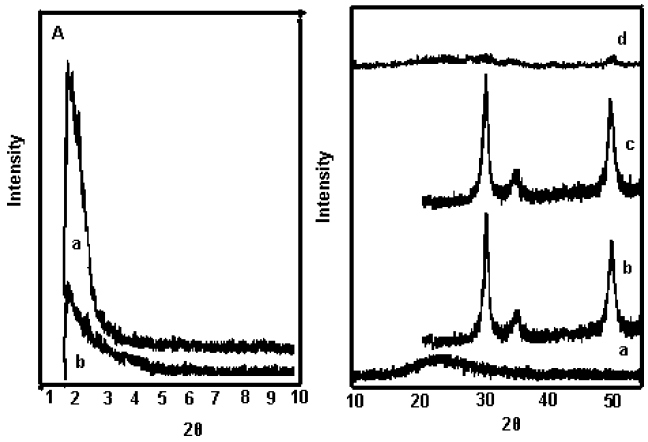

Figure 3. (A) XRD of (a) HMS and (b) UDCaT-6; (B) (a) HMS, (b) UDCaT-5, (c) S-ZrO_2, (d) UDCaT-6.

TABLE 1: BET Surface Area and Pore Size Analysis of HMS, S-ZrO_2, UDCaT-5, and UDCaT-6

catalysts	BET surface area (m^2/g^{-1})	pore volume (cm^3/g^{-1})	average pore diameter (Å)
HMS	1120	1.2	33
S−ZrO_2	100	0.11	20
UDCaT-5	83	0.11	20
UDCaT-6	870	0.70	32

3.1.3. BET Surface Area and Pore Size Analysis. The textural characterization of HMS and UDCaT-6 was performed by nitrogen BET surface area and pore size analysis (Table 1). Both HMS and UDCaT-6 display characteristic type IV adsorption isotherms (Figure 4) with well defined steps in N_2 adsorption and desorption isotherms and hysteresis in the desorption isotherm at relative pressures (p/p_0) in the range 0.45−0.8. This behavior is indicative of uniform meso pore sizes in both HMS and UDCaT-6 that are filled spontaneously due to capillary condensation. HMS retains its mesoporosity even after having been converted to UDCaT-6, and the explanation is in accordance with IUPAC classification.[32] Furthermore, UDCaT-6 displays fairly uniform pore size distribution centered at 32 Å and the average pore diameter of UDCaT-6 is reduced marginally to 32 Å from 33 Å of HMS (Table 1 and Figure 5); however, there was no broadening of the size distribution, indicating that the active centers of chlorosulfonic acid treated zirconia are uniformly dispersed inside the mesopores of HMS. The reduction in the BET surface area and pore volume of UDCaT-6 vis-à-vis HMS is much more remarkable in comparison to their respective pore sizes, indicating that nanoparticles of zirconia are generated in situ after treatment of chlorosulfonic acid and that some large particles can block a few pore junctions, thereby reducing accessibility of some channels of HMS. Thus, there is a reduction in surface area and pore volume of UDCaT-6. However, all of these values are far greater than those of bulk unsupported S-ZrO_2 and of UDCaT-5 (Table 1). Our results are in consonance with earlier literature reports.[33]

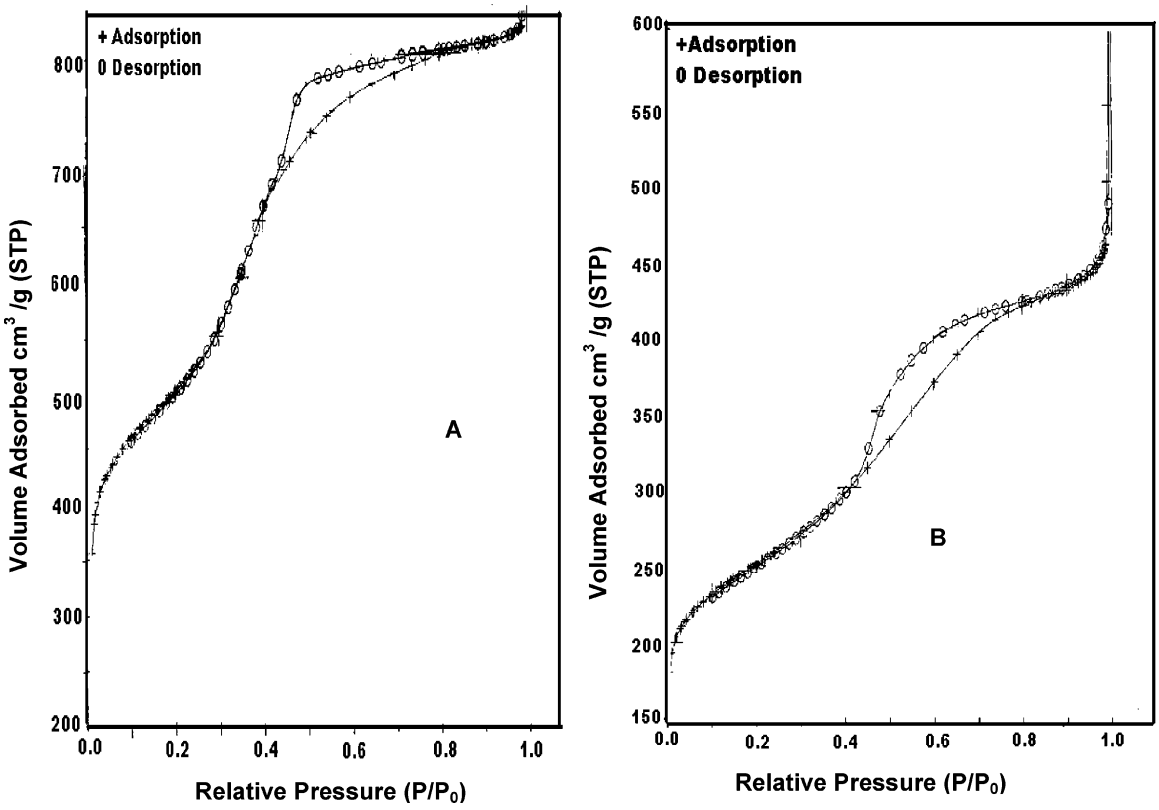

Figure 4. Adsorption isotherms: (A) HMS, (B) UDCaT-6.

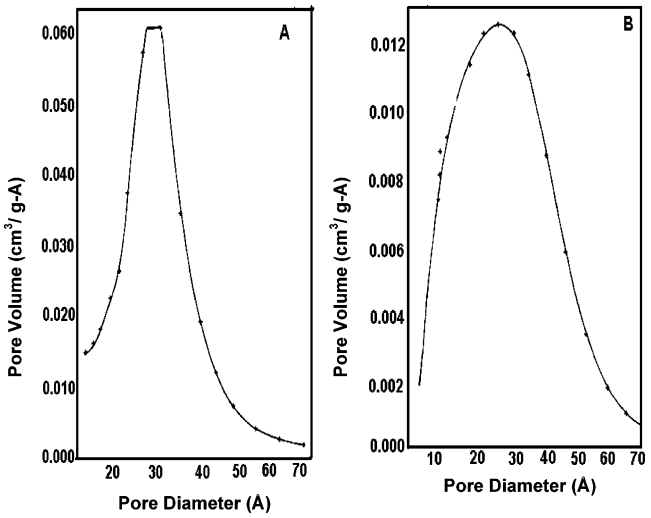

Figure 5. Pore size distributions: (A) HMS, (B) UDCaT-6.

XRD, BET surface area, and pore size analysis provide an explanation for entrapment of zirconia in mesoporous HMS. During the synthesis of UDCaT-6, the growth of crystalline zirconia is very unlikely because XRD data as well as BET surface area measurements indicate that the characteristic hexagonal structure of HMS and its mesoporosity are not perturbed in UDCaT-6, thus indicating framework stability. Growth of zirconia inside the HMS framework would have resulted in extensive damage of the framework and broadening of pore size distribution, which were not observed. Previous reports suggest that the intensity of the Bragg X-ray peak of mesoporous material at low angle is significantly dependent on the scattering material present inside the pores. Anderson et al.[34] found that the removal of surfactant by calcination was accompanied by a very large increase (by a factor of almost five) in the intensity of the most intense Bragg X-ray peak, in comparison with the uncalcined material. These results are in accordance with those of Marler et al.,[35] who have provided experimental evidence for a decrease in the X-ray Bragg intensities after filling the pores of calcined boron-substituted MCM-41 silica with various organic liquids. Pore filling by 1,2-dibromoethane, bromoform, and diiodomethane almost completely eliminated the (100) Bragg reflection. Recalcination to remove the organic adsorbent restored the (100) reflection to nearly its original intensity. Glinka et al.[36] have carried out neutron diffraction contrast studies on MCM-41 and observed that Bragg diffraction disappeared when the pores were filled with D_2O/H_2O mixtures that have the same scattering of cross-section as SiO_2. Edler and White[37] reported large changes in the Bragg intensities when MCM-41 silicas were dried for long periods. Furthermore, introduction of scattering material into the pores of HMS leads to an increased phase cancellation between scattering from the wall and the pore regions and therefore leads to reduced scattering intensities for the Bragg reflections at low angle ($2\theta = 1-7°$). The degree of cancellation is mainly determined by the scattering contrast between the framework walls and the pores.[38] Earlier literature suggests that the Bragg's intensity of mesoporous material below low angle is remarkably dependent on the scattering material present inside. Figure 3A shows the reduction of the typical (100) Bragg reflections of UDCaT-6 in comparison with HMS. Our results are in consonance with the past literature. This led us to corroborate that in UDCaT-6 nanoparticles of zirconia ($\ll$3.3 nm) must have formed inside the pores of HMS, and some of them are trapped at the pore junctions. Further, XRD patterns of both unsupported S-ZrO_2 and UDCaT-5 show the pure tetragonal phase of zirconia in the ordinary region. This lends credence to the conclusion that the tetragonal phase of zirconia must be trapped inside the pores of UDCaT-6. Impregnation of the aqueous salt of the zirconia precursor by incipient wetness technique into the pore space of HMS and subsequent hydrolysis

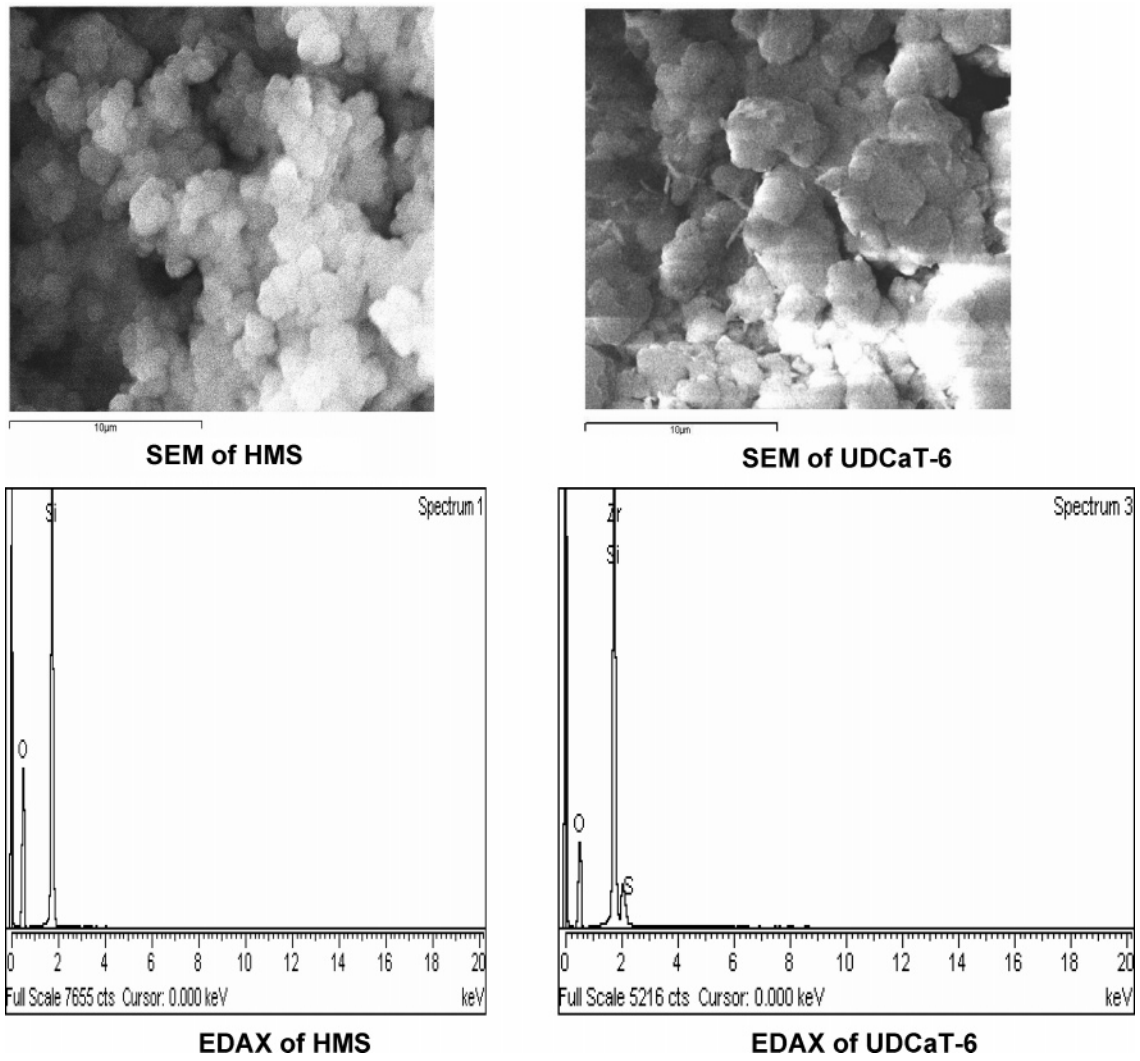

Figure 6. SEM and EDAX of HMS and UDCaT-6.

TABLE 2: EDAX of HMS and UDCaT-6

catalysts	elements	weight %	atomic %
HMS	O K	54.49	67.76
	Si K	45.51	32.24
total		100.00	
UDCaT-6	O K	41.23	60.23
	Si K	42.59	35.44
	S K	0.38	0.28
	Zr L	15.80	4.05
total		100.00	

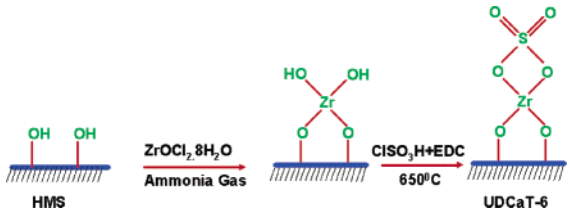

Figure 7. Conceptual mechanism for the formation of acid sites into UDCaT-6.

by ammonia gas result in precipitation of $Zr(OH)_4$ in mesopores of the HMS. As a result, once it is precipitated, it is very difficult for $Zr(OH)_4$ to come out from the pores of HMS during washing and drying. After treatment with chlorosulfonic acid and calcination at 650 °C, condensation of the hydroxyl group of $Zr(OH)_4$ occurs, leading to a crystalline zirconia without a change of nature of the sulfate species. FTIR and XRD spectra provide an explanation for these assumptions. Furthermore, the pore volume of UDCaT-6 is much less than that of pure HMS, indicating that large amounts of crystalline nanoparticles of zirconia are present inside the pores of UDCaT-6.

3.1.4. SEM and EDXS. SEM of HMS and UDCaT-6 (Figure 6 and Table 2) reveal that HMS is made up of sub-micrometer sized free-standing or aggregated sphere shaped particles.[39] A similar type of morphology is observed in UDCaT-6. The EDXS analysis shows the incorporation of zirconia and sulfur in UDCaT-6. It should be noted that sulfur Ka1 and zirconium La1 distribution spectra determined by SEM-EDXS analysis have clearly shown homogeneous distribution of S and Zr atoms in UDCaT-6. These results are in accordance with earlier literature reports.[33] SEM and EDXS analysis further supports the argument that active centers of chlorosulfonic acid treated zirconia are successfully embedded inside pores of HMS and that the structural integrity of the HMS is not altered even after it is converted to UDCaT-6.

We believe that this is a novel method for generation of active sites inside pores of catalytically inactive mesoporous material HMS by impregnating zirconia and treating it with chlorosulfonic acid as new source for sulfate ions, resulting in a novel catalyst UDCaT-6 (Figure 7).

3.2. Catalytic Activity and Stability of UDCaT-6. The activity, robustness, and reusability of solid acids should be tested in the presence of HCl and water in liquid and vapor phase reactions. The liquid phase benzylation of toluene with

TABLE 3: Activity of HMS, S-ZrO_2, UDCaT-5, and UDCaT-6 in Liquid Phase Alkylation of Toluene with Benzyl Chloride[a]

	catalysts			
parameter	HMS	S−ZrO_2	UDCaT-5	UDCaT-6
TON for benzylation of toluene with benzyl chloride[a]	0	96	185	933
selectivity	0	98%, mixture of benzylated toluene		

[a] Reaction Conditions: mole ratio of toluene/benzyl chloride, 10:1; speed of agitation, 1000 rpm; temperature, 90 °C; catalyst loading, 0.018 g/cc; reaction time, 1 h. TON (turnover number) = moles of product/moles of zirconia present in the catalyst.

TABLE 4: Activity of UDCaT-6 and Amberlyst-15 for Synthesis of TAME[a]

		product distribution	
catalysts	conversion %	yield of % (2MB2+2MB1)[b]	Yield of % TAME[c]
HMS	0	0	0
Amberlyst-15	98	96	4
S−ZrO_2	94	92	8
UDCaT-5	94	88	12
UDCaT-6	95	82	18

[a] Reaction conditions: mole ratio of *tert*-amyl alcohol/methanol, 1:5; WHSV = 20 h^{-1}; carrier gas, N_2; temperature, 120 °C. [b] Yield of 2MB2 + 2MB1 = amount of 2MB1 and 2MB2 formed/amount of *tert*-amyl alcohol reacted. [c] Yield of TAME = amount of TAME formed/amount of *tert*-amyl alcohol reacted.

benzyl chloride was used to evaluate the reactivity and stability of UDCaT-6, where corrosive HCl is evolved as a coproduct; it will be a good probe reaction to study the robustness of the catalyst.[3] Table 3 shows that UDCaT-6 gives an excellent turnover number in comparison with S-ZrO_2 and UDCaT-5 for the same reaction. The reusability of the catalyst was also tested thrice for benzylation of toluene to establish that there was no deactivation. These results confirmed that there was no leaching of the sulfate ion in the presence of HCl; thus, UDCaT-6 is a stable catalyst.

Vapor phase synthesis of TAME from *tert*-amyl alcohol and methanol was studied and compared with Amberlyst-15, S-ZrO_2, and UDCaT-5. As mentioned earlier, the stability of sulfated zirconia is susceptible where water is generated as a coproduct. When fresh sulfated zirconia is mixed with water, the pH of the suspension decreases quickly as a result of sulfate group hydrolysis that is confirmed by the identification of sulfate ions in the aqueous phase. A test for sulfate leaching was conducted for both fresh and reused UDCaT-6 by pH measurement,[40] and it was found that there was no leaching of sulfate ions. A similar phenomenon was observed in the case of UDCaT-5.[3c] The stability of UDCaT-6 on time-on-stream (TOS) was tested at 120 °C for 70 h. It was found that the conversion of TAA, yield of TAME, and selectivity toward TAME remained practically the same. The catalyst was thus stable. This further bolsters the earlier observations on the stability of UDCaT-6.

Additionally, in the case of the etherification of the *tert*-amyl alcohol with methanol, there is in situ generation of isoamylenes, namely, 2-methyl-1-butene (2MB1) and 2-methyl-2-butene (2MB2), via cracking of *tert*-amyl alcohol. Possible reactions are depicted in Scheme 1. A good cracking catalyst and a poor etherification catalyst would result in loss of the generated isoamylenes. A reverse phenomenon would result in poor yields of TAME. It was therefore necessary that the best catalyst should give a reasonable activity for the cracking of *tert*-amyl alcohol as well as the etherification of isoamylenes with methanol. UDCaT-6 gives excellent per pass yield of TAME compared to other catalysts (Table 4). Further, there was no formation of dimers of the alkenes. With both catalysts, *tert*-amyl alcohol dehydrates to give 2MB1 and 2MB2 and then reacts with methanol to give TAME; thus, equivalent moles of water is formed.

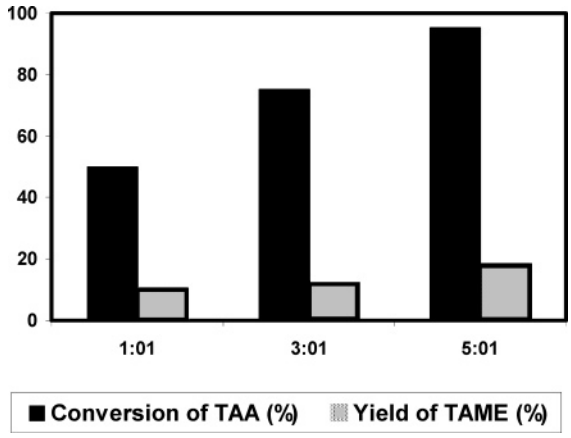

Figure 8. Effect of mole ratio of methanol to TAA on conversion and yield. W/F_{A_0}: 259.74 kg h mol^{-1}; Temp: 120 °C.

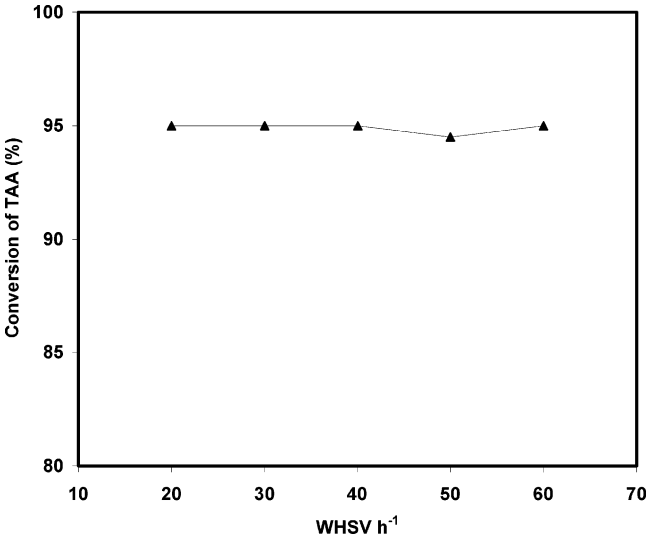

Figure 9. Assessment of mass transfer resistance. W/F_{A_0}: 259.74 kg h mol^{-1}; Temp: 120 °C.

3.3. Effect of the Mole Ratio of TAA to Methanol. The effect of the mole ratio of *tert*-amyl alcohol to methanol was studied in the range 1:1−1:5 (Figure 8). Both the conversion of t*ert*-amyl alcohol and the yield toward TAME increase with the increasing mole ratio of *tert*-amyl alcohol to methanol. As the concentration of methanol increases, the number of available sites for adsorption of *tert*-amyl alcohol decreases, and there is no further increase in conversion and yield above a mole ratio of 1:5.

3.4. Effect of External Mass Transfer. The influence of mass transfer resistance on conversion of mesitylene was assessed by increasing the carrier gas flow rate under otherwise similar conditions of temperature, space time of *tert*-amyl alcohol (W/F_{A_0}), and catalyst quantity at 120° C, 259.74 kg h mol^{-1}, and 2 g, respectively. Figure 9 indicates that there is no external mass transfer limitation.

A theoretical calculation was also done based on the Wiesz−Prater modulus to asses the influence of intraparticle diffusion resistance, according to which the value of $(-r_{obs}\rho_p R_p^2/D_e[A_s])$

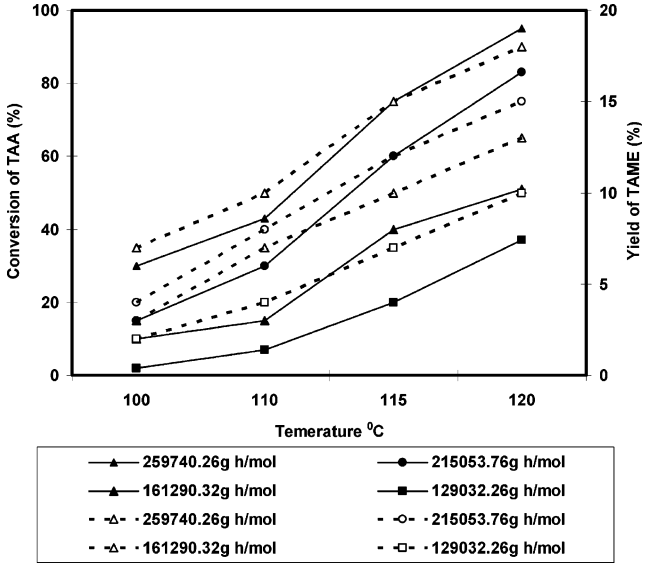

Figure 10. Effect of temperature on conversion of TAA and yield of TAME at different space times. Dashed lines: TAME yield (one pass). Solid lines: conversion (one pass). TAME yield = amt TAME formed/amt *tert*-amyl alcohol reacted.

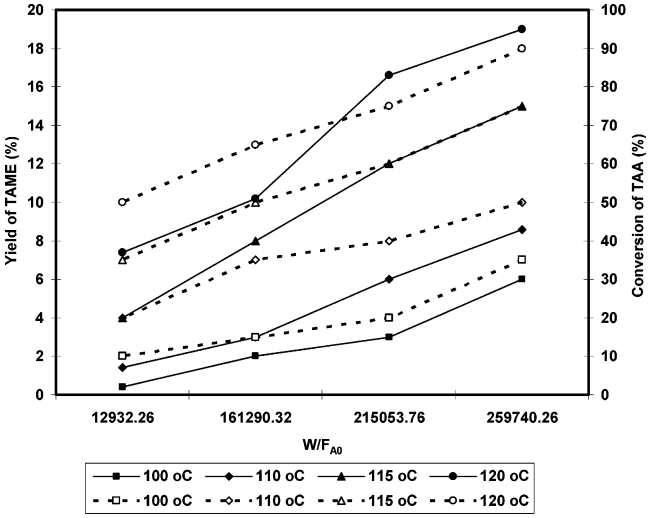

Figure 11. Effect of space time on conversion of TAA and yield of TAME at different temperatures. Dashed lines: TAME yield (one pass). Solid lines: conversion (one pass). TAME yield = amt TAME formed/amt *tert*-amyl alcohol reacted.

has to be far less than unity for the reaction to be intrinsically kinetically controlled. The calculated value of 2.5×10^{-8} demonstrates the absence of intraparticle resistance giving a catalyst effectiveness factor of unity. Thus, a WHSV of 20 h^{-1} was maintained constant during further experiments.

3.5. Effects of Temperature and Space Time. The effects of temperature on the conversion of *tert*-amyl alcohol (TAA) and yield of TAME were studied at a WHSV of 20 h^{-1}. With increasing temperature and space time, both conversion and yield were found to increase (Figures 10 and 11), which was due to increased contact time of the substrate on the catalyst surface. It also supported the earlier observations that the reaction was free from external mass transfer and intraparticle diffusion effects. The range of space velocities suggests that 259.74 kg h mol^{-1} is the optimum space time that gives 95% conversion of TAA and 18% yield toward TAME. There was no effect of temperature and space time on the selectivity of TAME, which remained the same at all temperatures and space times.

4. Development of Kinetic Model

The experimental observations, in the absence of external mass transfer limitations, show the following trends for the rate of reaction and selectivity of TAME:

(i) Rate of reaction is proportional to the partial pressure of TAA and the yield and selectivity of TAME remain constant for a given TAA feed rate and temperature.

(ii) Rate of reaction is proportional to partial pressure of methanol up to a certain value, beyond which it remains practically the same. The yield of TAME increases with the increasing partial pressure of methanol in the feed. It remains practically the same for a mole ratio of 5:1 of methanol to *tert*-amyl alcohol. There was no formation of dimethyl ether, even with increasing partial pressure of methanol.

(iii) Yields of the olefins, 2MB1 and 2MB2, which are dehydration products of TAA, are also proportional to the partial pressure of TAA in the feed. There was no dimerization or further oligomerization of 2MB1 and 2MB2 at all partial pressures of TAA or methanol.

(iv) Initial rate of reaction of TAA, and hence conversion of TAA and the yield of TAME, increases with increasing temperature at a fixed molar ratio of reactants; however, the yields of 2MB1 and 2MB2 decrease and the ratio of their yields in the outgoing stream is practically unaffected at all temperatures studied.

(v) Preliminary analysis of rate data showed that the reactants and products have lower boiling points and were weakly adsorbed at 120 °C and 1 atm pressure.

Based on the above observations, Scheme 1 was conceived and only reactions (a)−(d) were found to be relevant. The chemisorption of *tert*-amyl alcohol (A) and methanol (B) on a vacant site (S) gives surface species AS and BS. The chemisorbed species AS undergoes three parallel reactions to produce TAME (T) (from AS and BS), and 2MB1 and 2MB2 (from AS). The isomerization of 2MB1 to 2MB2 reaction is also likely to occur but is of no consequence. The reaction was carried out at 120 °C in the vapor phase, and it was found that through preliminary analysis of the data the adsorption terms were insignificant. Thus, the overall rate of reaction of *tert*-amyl alcohol (A) (mol/s·g-cat), assuming parallel reactions (a), (b), and (c) as rate controlling, is given by

$$-r'_A = (k_1 C_{BS} + k_2 + k_3) C_{AS} \tag{1}$$

The concentration C_S of the vacant sites (S) is calculated from the total sites (C_t), adsorption equilibrium constants (K_i), and concentration of the relevant species (C_i). Thus,

$$-r'_A = (k_1 K_B C_B + k_2 + k_3) K_A C_A \tag{2}$$

$$-r'_A = k' C_A \; when \; C_{B_0} \gg C_{A_0} \tag{3}$$

where the overall pseudoconstant for the reaction of A (k') is given by

$$k' = (k_1 K_B C_{B_0} + k_2 + k_3) K_A \tag{4}$$

For a fixed bed reactor with plug flow of vapors, where the mole ratio of methanol (B) is taken in far excess over *tert*-amyl alcohol (A), the total overall fractional yield ϕ of TAME

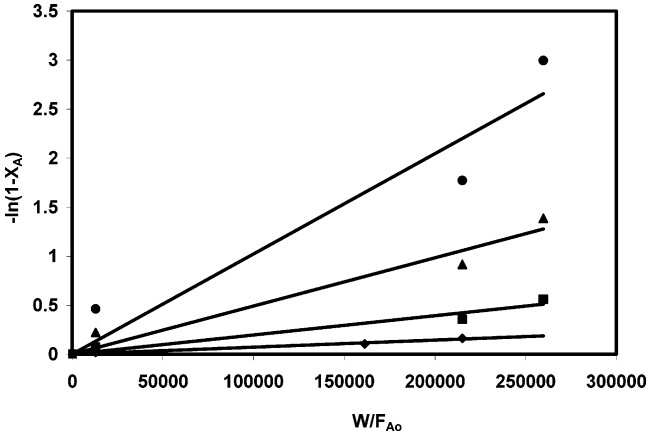

Figure 12. Pseudo-first-order plot: $-\ln(1 - X_A)$ vs W/F_{A_0} for synthesis of TAME. ◆ 100 °C; ■ 110 °C; ▲ 115 °C; ● 120 °C.

with reference to the amount of A reacted is obtained from the instantaneous yield as follows:

$$\psi = \phi = = \frac{k_1 K_B C_B}{k_1 K_B C_B + k_2 + k_3} = \frac{1}{1 + \dfrac{k_2 + k_3}{k_1 K_B C_B}} \qquad (5)$$

When $k_1 K_B C_B \ll k_2 + k_3$ then eq 5 reduces to

$$\psi = \phi = = \frac{k_1 K_B C_B}{k_2 + k_3} \qquad (6)$$

Eq 6 shows that the yield of TAME is independent of the concentration of A and should increase with the concentration of B.

On the contrary, when

$$k_1 K_B C_B \gg k_2 + k_3, \psi = \phi = 1 \qquad (7)$$

it will become independent of the concentration of B.

In the current studies, the yield of TAME was found to be independent of the concentration of A (*tert*-amyl alcohol), and it increased with methanol concentration at low values and was independent of concentration of methanol at higher concentrations. The yield was found to increase with increasing temperature for a fixed mole ratio of A and B, which is also according to the above eq 6.

The instantaneous combined yield of olefins 2MB1 and 2MB2 is given by

$$\psi_{MB} = \phi_{MB} = \frac{k_2 + k_3}{k_1 K_B C_B + k_2 + k_3} \qquad (8)$$

The combined yield of the olefins was found to be unaffected by the concentration of A and was independent at higher concentrations of B. These observations were taken as a valid proof of this kinetic model.

Now, eq 2 is integrated to get the following for a fixed bed vapor phase catalytic reactor:

$$-\ln(1 - X_A) = k' C_{A_0} \frac{W}{F_{A_0}} \qquad (9)$$

Thus, a plot of $-\ln(1 - X_A)$ versus W/F_{A_0} was made at different temperatures (Figure 12) to get a good *fit* up to 115 °C. However, the fit is not so good at 120 °C because the rate of reaction is very high and the reaction no longer remains a pseudo-first-order reaction. *Since there are substantial changes in the concentration of methanol at 120 °C due to much higher rates of reaction, the first term in eq 2 (that is, $k_1 K_B C_B K_A C_A$) is more predominant over others and the rate follows approximately second-order kinetics.*

The values of the rate constant (k') were calculated at different temperatures up to 115 °C and then an Arrhenius plot was made (not shown) to estimate the frequency factor and energy of activation. The values of the frequency factor and the apparent energy of activation were calculated to be 1.33×10^{19} $cm^3 mol^{-1} s^{-1}$ and 39 kcal mol^{-1}, respectively. This high value of activation energy also confirmed that the overall rate of reaction was not influenced by either external mass transfer or by intraparticle diffusion resistance, and that it was an intrinsically kinetically controlled reaction.

5. Conclusion

The current work has addressed for the first time the use of chlorosulfonic acid as a source of sulfate ion to treat zirconia on HMS to synthesize a novel catalyst UDCaT-6 that exhibits excellent catalytic activity and stability in both vapor phase synthesis of TAME and liquid phase alkylation reactions. A kinetic model was built up for synthesis of TAME that suggested that the reaction is intrinsically kinetically controlled. The model explains the observations very well. A time-on-stream study was conducted up to 70 h, and no drop in catalytic activity was observed. Thus, UDCaT-6 is a robust and novel catalytic material, and it can be used for a prolonged period of time without deactivation. A number of other reactions are being studied with this novel catalyst.

Acknowledgment. G.D.Y. acknowledges funding from the Darbari Seth Professorship Endowment and NMITLI program of the CSIR, New Delhi (2001-03).

Nomenclature

A	*tert*-amyl alcohol (TAA)
B	methanol
$[A_s]$	catalyst surface concentration of TAA (mol cm^{-3})
$[A_0]$	initial concentration of TAA (mol cm^{-3})
C_i	concentration of species *i* (mol cm^{-3}); can be expressed as partial pressure (atm)
C_{A_0}	initial concentration of A, mol/cm^3
C_{B_0}	initial concentration of B, mol/cm^3
D_e	effective diffusivity of A (cm^2 s^{-1})
F_{A_0}	molar flow rate of TAA (mol h^{-1})
k'	pseudo rate constant (cm^3 g $^{-1}$ s^{-1})
k_1	surface reaction rate constant for reaction of A with B
k_2	surface reaction rate constant for dehydration of TAA to 2MB1
k_3	surface reaction rate constant for dehydration of TAA to 2MB2
K_4	isomerization reaction equilibrium constant for 2MB1 to 2MB2
K_i	adsorption equilibrium constant for species *i*
$-r_i$	rate of reaction of species *i* (mol/s·g-cat)
$-r_{obs}$	observed rate of reaction (mol g $^{-1}$ s^{-1})
R_p	radius of catalyst particle (cm)
W	weight of catalyst (g)
X_i	fractional conversion of species *i*

Greek Letters

ρ_p	catalyst density (g cm^{-3})
ψ	instantaneous yield of product
ϕ	over fractional yield

References and Notes

(1) (a) Yadav, G. D.; Nair, J. J. *Microporous Mesoporous Mater*. **1999**, *33*, 1. (b) Kumbhar, P. S.; Yadav, G. D. *Chem. Eng. Sci*. **1989**, *44*, 2535. (c) Yadav, G. D.; Thorat T. S.; Kumbhar, P. S. *Tetrahedron Lett*. **1993**, *34* (3), 529. (d) Yadav, G. D.; Thorat, T. S. *Ind. Eng. Chem. Res.* **1996**, *35* (3), 721. (e) Yadav, G. D.; Thorat, T. S. *Tetrahedron Lett*. **1996**, *37*, 5405. (f) Yadav, G. D.; Pujari, A. A. *Green Chem.* **1999**, *1* (2), 69. (g) Yadav, G. D.; Nair, J. J. *J. Chem. Soc., Chem. Commun*. **1998**, 2369. (h) Yadav, G. D.; Nair, J. J. *Langmuir* **2000**, *16* (9), 4072−79. (i) Yadav, G. D.; Nair, J. J.; Narendra, V.; US Patent 6,177,596 B1; Jan. 23, 2001. (j) Yadav, G. D.; Nair, J. J. *Catal. Lett*. **1999**, *62* (1), 49−52.

(2) (a) Yadav, G. D.; Krishnan, M. S.; Pujari, A. A.; Doshi, N. S.; Mujeebur Rahuman M. S. M. U.S. Patent 6,204,424 B1 2001. (b) Yadav, G. D.; Pujari, A. A.; Joshi, A. V. *Green Chem.* **1999**, *1*, 269.

(3) (a) Yadav, G. D.; Murkute, A. D. *Adv. Synth. Cat*. **2004**, *346*, 389. (b)Yadav, G. D.; Murkute, A. D. *Langmuir*, in press. (c) Yadav, G. D.; Murkute, A. D. *J. Catal*. **2004**, *224*, 218.

(4) Päivi, K.; Pääkkönen, A.; Outi Krause I. *React. Funct. Polym*. **2003**, *55*, 139.

(5) Oosta, C.; Hoffmann, U. *Appl. Catal., A* **1996**, *51*, 329.

(6) Matouq, M. H.; Goto, S. *Int. J. Chem. Kinet*. **1993**, *25*, 825.

(7) Matouq, M. H.; Tagawa, T. Goto, S. *J. Chem. Eng. Jpn*. **1993**, *26*, 254.

(8) Yin, X. D.; Yang, B. L.; Goto, S. *Int. J. Chem. Kinet*. **1995**, *27*, 1065.

(9) Yadav, G. D.; Joshi, A. V. *Org. Process Res. Dev*. **2001**, *5*, 408.

(10) Yadav, G. D.; Bokade, V. V. *Appl. Catal., A* **1996**, *147* (2) 299.

(11) Yadav, G. D.; Kirthivasan, N. In *Fundamental and Applied Aspects of Chemically Modified Surfaces*; Blitz, J. P., Little, C. B. Eds.; Royal Society of Chemistry: 1999; pp 254−269.

(12) Yadav, G. D.; Kirthivasan, N. *J. Chem. Soc., Chem. Commun*. **1995**, 203.

(13) Yadav, G. D.; Kirthivasan, N. *Appl. Catal., A* **1997**, *154*, 23.

(14) Yadav, G. D.; Krishnan, M. S. *Ind. Eng. Chem. Res*. **1998**, *27* (8), 3358.

(15) Harmer, M. A.; Sun, Q. *Appl. Catal., A* **2001**, *221*, 45.

(16) Sharma, M. M. *React. Polym*. **1995**, *22*, 1−21.

(17) Chakrabarti, A.; Sharma, M. M. *React. Polym*. **1993**, *20*, 1.

(18) Hutchings, G. J.; Nicolaides, C. P.; Scurrell, M. S. *Catal. Today*. **1992**, *15*, 23.

(19) Le Van Mao, R.; Le, T. S.; Faibairn, M.; Muntasar, A.; Xiao, S.; Denes, S. *App Catal., A* **1999**, *185*, 221.

(20) Collignon, F.; Mariani, M.; Moreno, S.; Remy, M.; Poncelet, G. *J. Catal*. **1997**, *166*, 53.

(21) Nikolopoulos, A. A.; Kogelbauer, A.; Goodwin, J. G. Jr.; Marcelin, G. *Catal. Lett*. **1996**, *39*, 173.

(22) Kim, J. S.; Kim, J. M.; Seo, G.; Park, N. C.; Niiyama, S. *Appl. Catal., A* **1988**, *37*, 45.

(23) Adams, J. M.; Martin, K.; McCabe, R. W.; Murray, S. *Clays Clay Miner*. **1986**, *34*, 597.

(24) Quiroga, M. E.; Figoli, N. S.; Sedran, U. A. *J. Chem. Eng*. **1997**, *67*, 199.

(25) Chu, P.; Kühl, G. H. *Ind. Eng. Chem. Res*. **1987**, *26*, 365.

(26) Nikolopoulos, A. A.; Oukaci, R.; Goodwin Jr. J. G.; Marcelin, G. *Catal. Lett*. **1994**, *27*, 149.

(27) Le Van.; Mao, R.; Carli, R.; Ahlafi, H.; Ragaini, V. *Catal. Lett*. **1990**, *6*, 321.

(28) Collignon, F.; Leonders, R.; Martens, J. A.; Jacobs, P. A.; Poncelet, G. *J. Catal*. **1999**, *182*, 302.

(29) Tanev, P. T.; Pinnavaia, T. J. *Science* **1995**, *267*, 865.

(30) *Kirk-Othmer Encyclopedia of Chemical Technology*, 4th Edition; 1993; Vol. 6, p 168.

(31) Ward, D. A.; Ko, E. I. *J. Catal*. **1994**, *150*, 18.

(32) Sing, K. S. W.; Everett, D. H.; Haul, R. A. W.; Mouscou, L.; Pierotti, R. A.; Rouquerol, J.; Siemieniewska, T. *Pure. Appl. Chem*. **1985**, *57*, 603.

(33) Xia, Q. H. Hidajat, K. Kawi, S. *J. Catal*. **2002**, *205*, 318.

(34) Anderson, M. T.; Martin, J. E.; Odinek, J.; Newcomer, P. In *Access in Nanoporous Materials*, Pinnavaia, T. J., Thorpe M. F., Eds.; Plenum Press: New York, 1995; p. 29.

(35) Marler, B.; Oberhagemann, U.; Vortmann, S.; Gies, H. *Microporous Mater*. **1996**, *6*, 375.

(36) Glinka, C. J.; Nicol, J. M.; Stucky, G. D.; Ramli, E.; Q. Margolese; Huo, J. B.; Higgins, M. E.; Leonowicz, *J. Porous Mater*. **1996**, *3*, 93.

(37) Edler, K. J.; White, J. W. *J. Chem. Soc., Chem. Commun*. **1995**, 155.

(38) Hammond, W.; Prouzet, E.; Mahanti, S. D.; Pinnavaia, T. J. *Microporous Mesoporous Mater*. **1999**, *27*, 19.

(39) Mokaya, R.; Zhou, W.; Jones, W. *J. Mater. Chem*. **2000**, *10*, 1139−1145.

(40) Omota, F.; Dimian, A. C.; Bliek, A. *Chem. Eng. Sci*. **2003**, *58*, 3175.